Functional Polymer Brushes on Diamond as a Platform for Immobilization and Electrical Wiring of Biomolecules

*Andreas A. Reitinger, Naima A. Hutter, Andreas Donner, Marin Steenackers, Oliver A. Williams, Martin Stutzmann, Rainer Jordan, and Jose A. Garrido**

For the biofunctionalization of electronic devices, polymer brushes can provide a route which allows combining the advantages of other commonly used approaches, such as immobilization of functional biomolecules via self assembled monolayers or coated polymer matrices: high stability and loading capacity, efficient electron transport, and excellent biocompatibility. In the work presented here, poly(methacrylic acid) brushes are prepared by self-initiated photografting and photopolymerization on diamond electrodes. In this straightforward process no prior grafting of initiators is required since the initiation of the polymerization can be conveniently controlled by the hydrogen or oxygen termination of the diamond surface. Boron doped nanocrystalline diamond as an electrode material provides extreme chemical inertness and stability, inherent biocompatibility, and superior electrochemical properties, such as the large accessible potential window and low background currents. As a proof of concept we demonstrate the amperometric detection of glucose by polymer brushes covalently modified with the redox enzyme glucose oxidase and aminomethyl ferrocene as electron mediator. Characterization by X-ray photoelectron spectroscopy and atomic force microscopy both indicate a high loading of the ferrocene mediator. Consistently, electrochemical cyclic voltammetry shows a multilayer equivalent loading of ferrocene and highly efficient electron transfer throughout the polymer film. Overall, functionalized polymer brushes can provide a promising platform for the immobilization and electrical wiring of biomolecules for bioelectronic and biosensing applications.

1. Introduction

Through advances in both material growth and doping as well as surface functionalization techniques, nanocrystalline diamond (NCD) thin films have become a promising electrode material for bioelectronic applications.[1,2] In this field, not only the extreme durability and chemical inertness of diamond but also the large electrochemical window of around 3.5 V and the inherent biocompatibility of this carbon allotrope are of particular interest.[3,4] Commonly, functional biomolecules such as enzymes are either immobilized directly onto the electrode surface or embedded into a polymer matrix applied by some coating process from solution.[5,9] While the first approach ideally allows for an efficient charge transfer between biomolecule and electrode, the second one requires some sort of mediator to enable charge transport through the polymer film, but at the same time can provide a higher load of biomolecules per area.[10,11]

Polymer brushes prepared by self-initiated photografting and photopolymerization (SIPGP) on the diamond surface offer an intermediate strategy. As illustrated in **Scheme 1**, no polymerization initiator or extensive surface pretreatment is required, but still the polymer brushes can be patterned by mere control of the diamond surface termination.[12,13] Furthermore, surface patterning by carbon templating (e-beam induced carbon deposition and consecutive SIPGP) enables the control of the grafting density on any arbitrary substrate at the nanometer scale.[14–19] Biomolecules can be immobilized in these brushes by covalent coupling with the suitable coupling chemistry.[10–12] In this soft environment, proteins and enzymes are more likely to retain their structure and functionality as compared to a direct interaction with the diamond surface.[20,21] For bioelectronic applications, an electrical connection between the biomolecules and the electrode surface has to be established. Since typical polymer backbones exhibiting sufficient stability are nonconductive, charge transport mediators have to be introduced to the system.[22] Free mediator molecules in solution are impractical for several reasons, in particular for bio-applications (e.g., diffusion-limited charge transport, limited stability, reduced biocompatibility, unspecific background reactions), while intrinsically

A. A. Reitinger, A. Donner, Prof. M. Stutzmann, Dr. J. A. Garrido
Walter Schottky Institut
Physik-Department
Technische Universität München
Am Coulombwall 4, 85748 Garching, Germany
E-mail: garrido@wsi.tum.de
Dr. N. A. Hutter, Dr. M. Steenackers
Wacker-Chair of Macromolecular Chemistry
Chemie-Department
Technische Universität München
Lichtenbergstraße 4, 85748 Garching, Germany
Dr. O. A. Williams
Cardiff School of Physics and Astronomy
Queen's Buildings, The Parade, Cardiff CF24 3AA, UK
Prof. R. Jordan
Professur für Makromolekulare Chemie
Fachrichtung Chemie und Lebensmittelchemie
Technische Universität Dresden
Zellescher Weg 19, 01062 Dresden, Germany

DOI:10. 1002/adfm.201202342

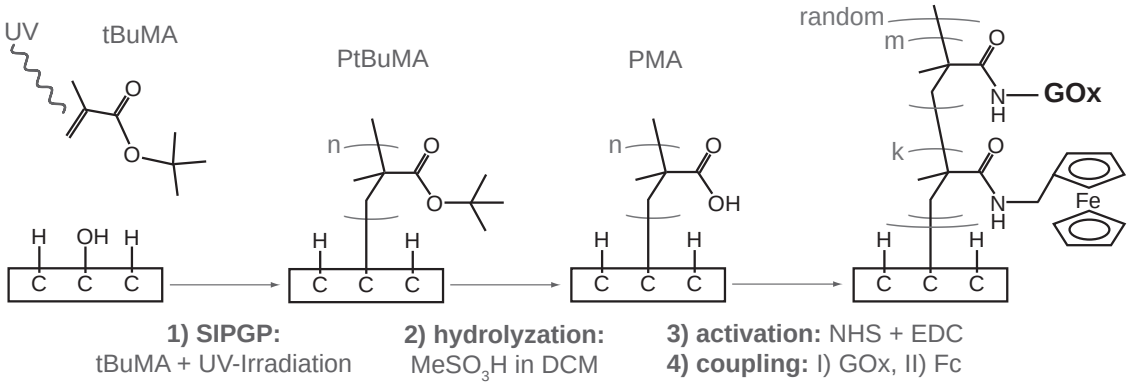

Scheme 1. 1) Self-initiated photografting and photopolymerization of tert-butyl methylacrylate on OH-terminated diamond. 2) Hydrolyzation of tert-butyl groups. 3) Activation of carboxyl groups. 4) Coupling of glucose oxidase and aminomethyl ferrocene.

conducting (e.g., conjugated) polymers often suffer from low stability. Hence, taking advantage of the versatility of polymer chemistry, we chose a dual functionalization of the polymers with biomolecules and electron mediators.

From the large variety of possible combinations of polymers, biomolecules, and mediators we chose the combination of glucose oxidase and aminomethyl ferrocene immobilized in poly(methacrylic acid) (PMA) brushes on diamond electrodes as an exemplary system to demonstrate the amperometric detection of glucose, and such the feasibility of our approach. PMA is a hydrophilic, readily synthesized, and biocompatible polymer well suited for SIPGP. On the other hand, glucose oxidase is a well studied, commercially available redox enzyme with promising medical applications, e.g., glucose sensing.[23–25] In our work, glucose oxidase (GOx) and aminomethyl ferrocene (Fc) are both immobilized via amide bonds along PMA, which was polymerized from the oxygen-terminated surface of a NCD electrode, as illustrated in **Scheme 2**c. When operated in an aqueous environment, GOx can catalyze the oxidation of β-D-glucose in solution to gluconolactone. In vivo, the two electrons are transferred via the FAD cofactor to O_2 and H_2O_2 is produced. In an oxygen-free environment (degassed electrolyte), the electrons can be transferred to a mediator molecule with suitable redox potential–in this case ferrocene. Charge transport between adjacent Fc molecules allows the electrons to reach the surface of the electrode which is set to a properly oxidizing bias (Scheme 2a). Finally, monitoring the generated electric current allows the detection of glucose.

2. Results and Discussion

2.1. Sample Preparation and AFM Characterization

Poly(methacrylic acid) brushes were prepared by self-initiated photografting and photopolymerization of *tert*-butyl

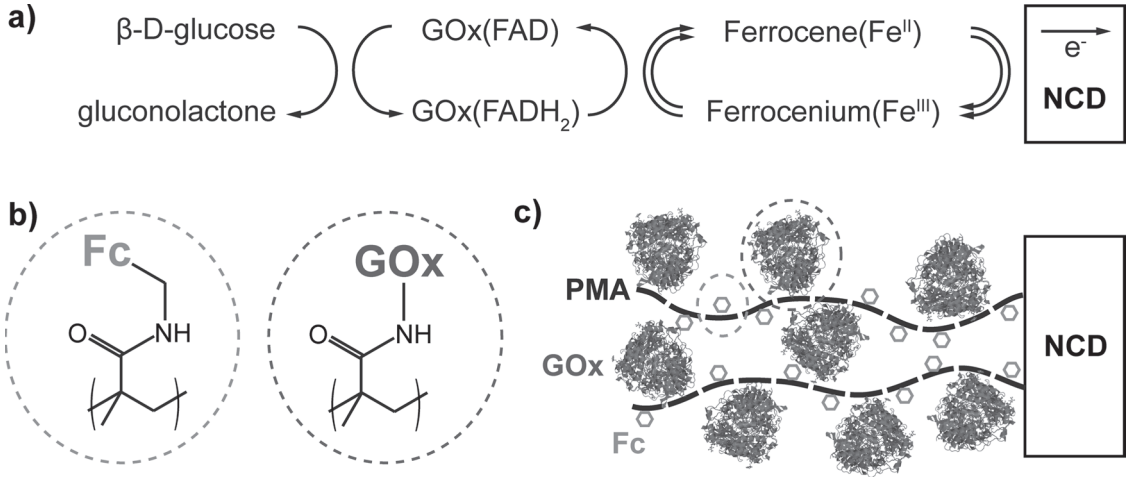

Scheme 2. a) Electron transport path from glucose oxidase (GOx) over several ferrocene (Fc) mediators to the diamond electrode. b) Fc and GOx coupled to poly(methacrylic acid) (PMA) through amide bonds. c) Fc-functionalized PMA brushes provide both mechanical and electrical connection to the diamond surface for the immobilized enzymes and allow a high loading of enzymes per surface area.

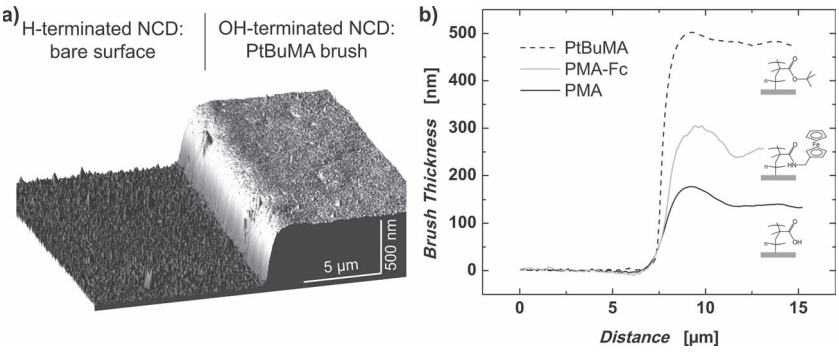

Figure 1. a) 3D topographic AFM image of a structured polymer brush (in PtBuMA stage) on nanocrystalline diamond with a pattern of hydrogen- and oxygen/hydroxyl-termination, revealing the high selectivity of the polymerization initiation towards the OH-terminated part of the NCD surface. b) AFM profiles measured in ambient air across the same brush in consecutive stages: after SIPGP of PtBuMA, after hydrolysis of protection group, and after coupling of Fc.

methylacrylate on oxygen-terminated, boron-doped nanocrystalline diamond surfaces, as illustrated in Scheme 1 (see also the Experimental Section). After polymerization, the *tert*-butyl protection group was removed by hydrolyzation to expose the carboxylic acid group, which increases the hydrophilicity of the polymer and allows the coupling of functional molecules via amide bonds. The thickness of the polymer brushes after polymerization, deprotection and functionalization was measured by atomic force microscopy on the structured sample shown in **Figure 1**a. The removal of the *tert*-butyl groups and branched material reduces the original brush height by 70%, as revealed in Figure 1b. Subsequent coupling of aminomethyl ferrocene increases the brush height by approximately 80%. It can be assumed that PtBuMA and PMA-Fc brushes are close to fully collapsed in ambient air, while for the PMA brushes the incorporated water in this rather hydrophilic polymer probably leads to a higher apparent profile, which would result in an underestimation of the Fc content.

2.2. Analysis of Brush Composition by XPS

To validate the presence of ferrocene in the polymer brushes and to better quantify the coupling efficiency, X-ray photoelectron spectroscopy (XPS) was performed. **Figure 2** shows the survey scans and detailed scans of the iron 2p peaks for pure PMA brushes as well as Fc-modified brushes. Due to spin-orbit coupling and the different oxidation states of the iron atom in ferrocene (Fe^{II}) and ferrocenium (Fe^{III}) two peak doublets occur in the high resolution scan of the Fe2p region in Figure 2b. The individual peaks were integrated based on the shown fits after Shirley background subtraction.[26] The position of the $Fe^{II}2p_{3/2}$ spectral line at 707.6 eV is in good agreement with tabulated values of 707.7 eV.[27] High resolution scans of the other peaks as well as more details of the data analysis can be found in the Supporting Information.

For the carbon, oxygen, and nitrogen 1s peaks as well as the iron 2p and 3p peaks the integrated peak areas were normalized by their respective relative sensitivity factors documented in the Supporting Information.[28,29] For the discussion below, it is worth recalling that the polymer brushes are thick and dense enough that contributions from the diamond substrate are negligible, which was confirmed by a control experiment on silicon. Consequently, the observed ratios of elements are representative for the composition and modification of the polymer brushes.

The theoretically expected and experimentally measured ratios of elements for pure and Fc-modified PMA brushes are summarized in **Table 1**. Pure PMA brushes, for example, are expected to have a ratio of carbon to oxygen of 2:1 and no nitrogen or iron (4 carbon and 2 oxygen atoms per monomer) while brushes of which all MA monomers are modified with aminomethyl ferrocene would be composed of 15 carbon atoms (4 from MA and

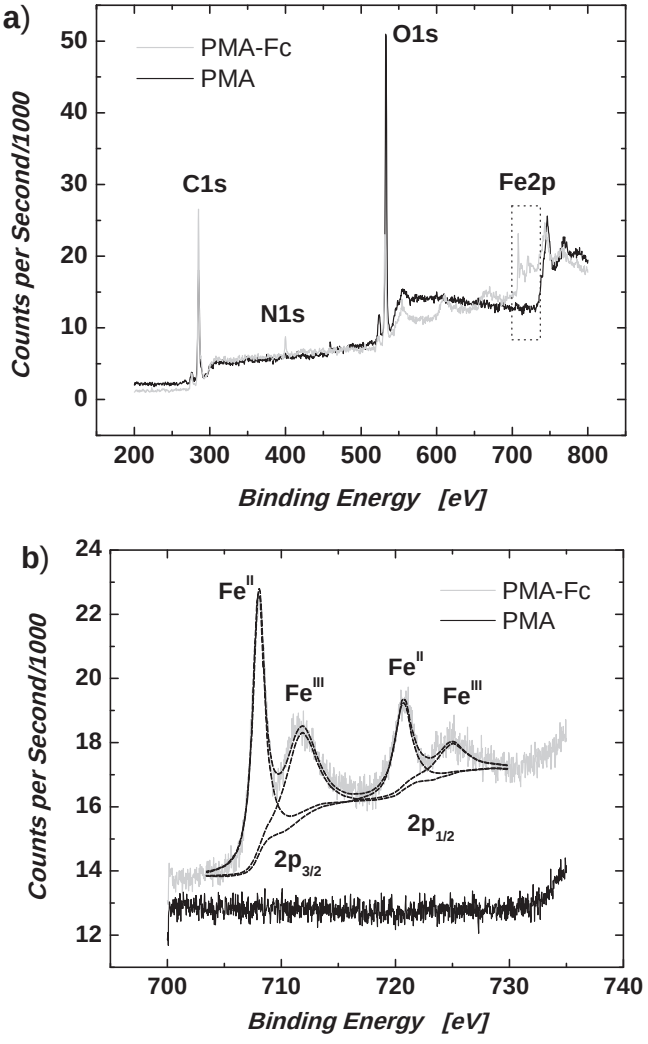

Figure 2. a) Survey scan of pure PMA and Fc-modified PMA on NCD. b) Two peak doublets in the Fe2p scan occur due to spin-orbit coupling and the different oxidation states of the iron atom in ferrocene (Fe^{II}) and ferrocenium (Fe^{III}). Peak integration (dashed lines) was done based on the shown peak fits and Shirley background subtraction.

Table 1. Relative amounts of elements normalized by the number of carbon atoms per monomer

	Carbon	Oxygen	Nitrogen	Iron
PMA theoretical	4	2	0	0
PMA experimental	4	3.7	0.1	0.0
PMA-Fc theoretical	15	1	1	1
PMA-Fc experimental	15	4.4	1.0	0.7

11 from aminomethyl ferrocene) and one oxygen, one nitrogen, and one iron atom per monomer.

The experimental data shows higher than expected oxygen contents which can be attributed to residual water in the polymer brushes. Due to this limitation, the oxygen amount can give no reliable information on the composition of the polymer brushes. However, iron- and nitrogen-to-carbon ratios suggest a grafting efficiency of aminomethyl ferrocene of 70% or higher.

2.3. Verification of Enzyme Activity

In order to verify the presence and determine the activity of GOx in PMA-GOx and PMA-Fc-GOx samples, a homovanillic acid (HVA) assay was applied.[30] A transparent cuvette was filled with a buffered solution of known concentrations of HVA, horseradish peroxidase (HRP), and glucose and placed in a photospectrometer. As soon as a sample containing active GOx is immersed in the solution, the following multistep reaction occurs: 1) Glucose oxidation is catalyzed by GOx leading to the formation of hydrogen peroxide; 2) Hydrogen peroxide is reduced by HRP to OH^-; 3) The oxidized HRP enzyme is reduced by HVA which is fluorescent in its oxidized dimeric form.

This was repeated for each sample at different glucose concentrations, but otherwise constant conditions and the fluorescence intensity (FI) was recorded over time. The FI is proportional to the concentration of oxidized HVA, and the same holds for the respective time derivatives. Consequently, the increase in FI over time is proportional to the number of active enzymes. To avoid a quantification model relying on optical absorption coefficients and enzyme kinetic parameters, the assay was calibrated by a control experiment using a solution of known GOx concentration (3.1 nM).

The plot in **Figure 3**a shows the typical hyperbolic behavior of an enzymatically catalyzed reaction for the functionalized samples and the control experiment, which can often be described by Michaelis–Menten kinetics.[31] Normalizing the activity of the PMA-GOx-Fc by the activity of the free GOx yields a surface concentration of 1.2×10^{11} molecules per cm^2, which corresponds to only about 8% of a densely packed monolayer. This is in contradiction with AFM measurements which reveal a multilayer loading of enzymes in the PMA brushes, as shown in Figure 3b for the case of polymer brushes modified with horseradish peroxidase. A detailed description of the preparation of similar samples can be found elsewhere.[12,13] The activity normalization described above assumes that every immobilized enzyme exhibits the same activity as free enzymes and that there are no constraints on diffusion. However, due to the coupling of the enzymes via their amino groups the orientation of enzymes towards the polymer strands is quasi random, and multiple bonds per enzyme could reduce enzymatic activity or (partially or fully) block the active site of unfavorably oriented enzymes. In addition, the dense PMA-GOx brushes could strongly hinder diffusion of the molecules involved in the assay, such that their concentration in the brushes could significantly deviate from that of the bulk solution. As a result, limited diffusive transport in the films would lead to an underestimation of the number of immobilized enzymes. Thus, the above calculated surface coverage only represents a lower bound.

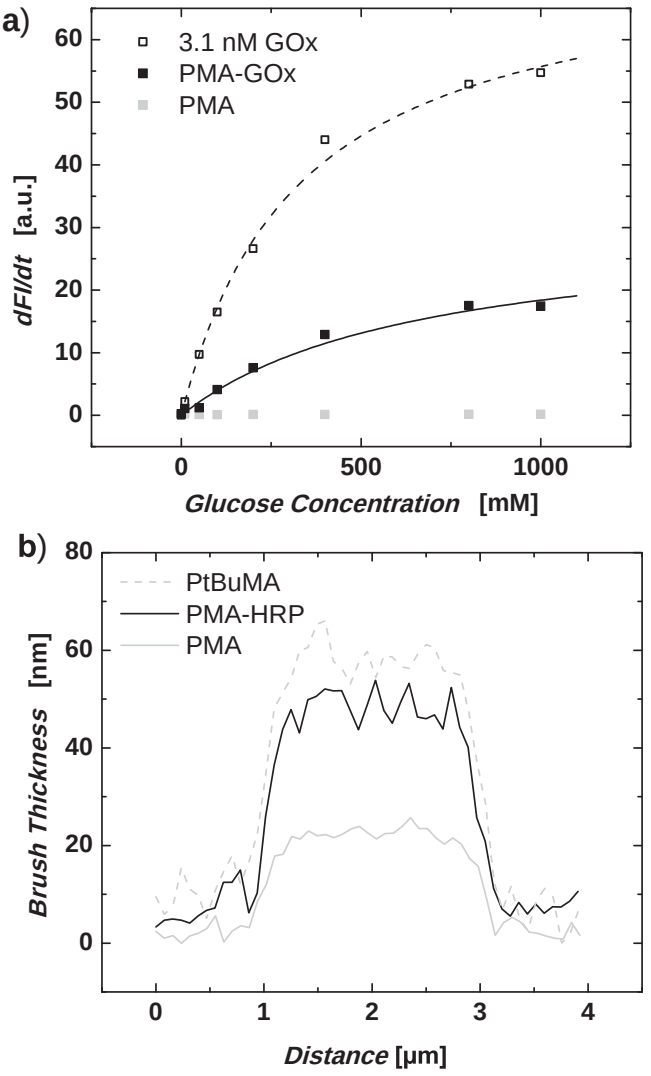

Figure 3. a) Rates of fluorescence intensity increase vs β-D-glucose concentration for pure PMA, PMA-GOx, and 3.1 nM free GOx derived from the HVA activity assay as described in the main text. Solid and dashed lines correspond to hyperbolic fits based on Michaelis–Menten kinetics. b) AFM height profiles of a patterned brush before and after removal of the tert-butyl group, and after coupling of horseradish peroxidase.

2.4. Electrochemical Characterization of Electron Transport

So far we could establish the successful grafting of PMA, its functionalization with Fc and GOx, as well as an estimation

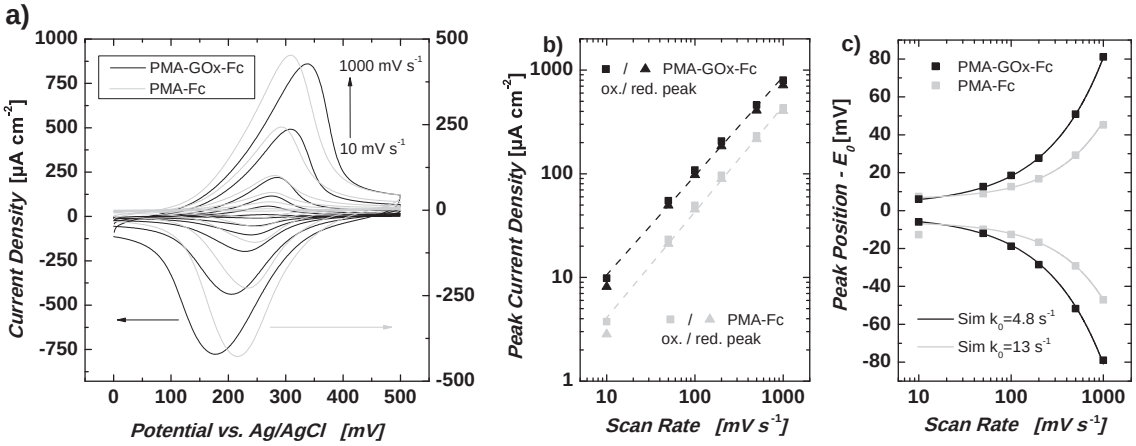

Figure 4. a) Cyclic voltammograms of a PMA-Fc and a PMA-GOx-Fc sample at scan rates ranging from 10 to 1000 mV s^{-1}, recorded in 10 mM PBS with 2.7 mM KCl and 137 mM NaCl; pH 7.4 at 25 °C. Notice the two different y-axes. b) Peak current densities (background subtracted) vs scan rate exhibit an almost linear dependence. c) Peak positions relative to the formal potential E^0 and Butler-Volmer simulations for fixed k^0 including a non-kinetic offset of peak separation (UQR).

of the activity of the immobilized enzymes, using XPS, AFM, and the HVA assay. To complement the quantification of the Fc amount and to study the efficiency of the electron transfer in the polymer, PMA brushes containing Fc as well as both Fc and GOx were investigated using cyclic voltammetry (CV). In CV the voltage applied between the (functionalized) working electrode and a reference electrode is swept at a constant rate between two potentials while the current is recorded. **Figure 4**a shows CVs of a PMA-Fc and a PMA-Fc-GOx sample at scan rates ranging from 10 to 1000 mV s^{-1}. For the PMA-Fc sample, peak integration after background subtraction and normalization by the scan rate yields a total amount of transferred charge of 49 ± 5 µC cm^{-2}, which corresponds to approximately 3.0 ± 0.3 Fc molecules per nm^2. For the PMA-GOx-Fc sample we obtained 79 ± 8 µC cm^{-2} corresponding to 4.9 ± 0.5 molecules per nm^2. For comparison, the theoretical maximum packing density of a monolayer of ferrocene is 2.8 molecules per nm^2 (based on a ferrocene diameter of 0.64 nm and hexagonal packing).[32] The counter-intuitively larger loading of Fc for the PMA-GOx-Fc sample in comparison to the PMA-Fc sample can be explained by variations between samples in PMA grafting density or brush thickness. These are caused by the variation in surface properties of different batches of NCD substrates and variations in polymerization parameters. However, under well controlled polymerization conditions the variations in brush thickness between samples within the same batch are significantly smaller (below 20%). Using the AFM profiles of structured, but otherwise similar PMA brushes, we can obtain a rough estimate of the polymer grafting density on the diamond surface. Considering an average length of 250 nm, with one Fc unit per monomer, a length of each monomer of approximately 1 nm, and the total amount of transferred charge determined above, for the PMA-GOx-Fc sample we estimate a grafting density of 0.02 PMA strands per nm^2 which is equivalent to a average distance of about 7 nm between the polymers on the surface.

Figure 4b shows peak current densities (background currents subtracted) vs. scan rate for both samples in a double logarithmic plot. In the case of charge transfer between the electrode and surface bound redox molecules a linear dependence would be expected, whereas for redox species in solution the diffusion-limited charge transfer should result in a square root dependence.[33] Fitting the data with a simple power function $y = c \times x^n$ yields exponents of $n = 0.94$ for the PMA-Fc sample and $n = 0.85$ for the PMA-GOx-Fc sample. The behavior of the PMA-Fc sample is in good accordance with the efficient charge transfer observed for surface bound redox species. On the other hand, for the sample containing also GOx, the charge transfer characteristics are slightly shifted towards a more diffusion-limited behavior. Overall, in comparison to other systems where mediators are immobilized in polymer matrices which commonly exhibit a clearly diffusion-limited behavior ($n = 0.5$), we observe a behavior more similar to tightly surface-bound redox species.[34–35]

The background-corrected CVs were fitted by simulated CVs based on Butler–Volmer theory to extract the standard heterogeneous rate constant k^0 and the transfer coefficient α. The non-zero peak separation at low scan rates, also termed unusual quasi-reversibility, is accounted for by a constant non-kinetic contribution ΔE_{UQR} to the observed peak separation ΔE_p.[36] Figure 4c shows the scan rate dependent positions of the oxidation and reduction peak minus the formal potential E^0 and simulations of the peak positions assuming a constant k^0. For the PMA-Fc and PMA-GOx-Fc sample formal potentials of 263 ± 3 mV and 257 ± 3 mV were determined, respectively. Transfer coefficients of 0.47 ± 2 for both samples indicate a high degree of reversibility of the oxidation and reduction of the immobilized Fc. Simulations using $k^0 = 13$ s^{-1} and $k^0 = 4.8$ s^{-1} as well as $\Delta E_{UQR} = 10.9$ mV and $\Delta E_{UQR} = 8.6$ mV, respectively, reproduced the observed peak positions accurately. However, there is a significant deviation of the observed peak shape (e.g., larger FWHM) from the ideal case of the simulated CVs (see

supporting information). Hence, the determined rate constants should be regarded as apparent rate constants, describing electron transfer kinetics of a more complex system with probably a distribution of actual rate constants. The larger ΔE_p (or smaller k^0) observed for the PMA-GOx-Fc in comparison to the PMA-Fc sample indicates a less efficient charge transfer which could be explained by an on average larger separation of Fc molecules due to the presence of GOx.[37,38]

2.5. Amperometric Detection of Glucose

Polymer brushes modified with GOx and Fc were used to investigate the amperometric detection of glucose. In this experiment a constant bias of +0.4 V vs Ag/AgCl (3 M KCl) was applied to the functionalized diamond electrode. After an equilibration time, increasing amounts of glucose were added to the electrolyte while the current was recorded. To reduce noise, the solution was stirred for one minute after adding glucose and then measured without perturbation for another 5 min. In **Figure 5**a, the sample containing GOx and Fc shows a clear response to the increasing glucose concentration in comparison to the sample containing only Fc. The plot of peak current density vs. glucose concentration shows, similar to the HVA assay, a hyperbolic dependence, as can be seen in Figure 5b. In principle, this is expected for an enzyme-catalyzed reaction and can be described by Michaelis–Menten kinetics. Then, the kinetic parameters $v_{max} = 78$ nA cm^{-2} and $K_M = 16$ mM can be extracted from the fit ($y = v_{max} \times x/(x + K_M)$, y being the current density and x the glucose concentration). However, when we calculate the amount of GOx using a catalytic rate constant $k_{cat} = 500$ s^{-1} for GOx, similarly to the HVA assay, we significantly underestimate the surface coverage to only 9.7×10^8 enzymes per cm^2.[39] As discussed already for the HVA assay, this suggests again that a lower k_{cat} for the immobilized enzymes in combination with hindered diffusion of educts and products through the polymer brushes could limit the performance of our system. This is supported by the observation that after the glucose concentration is increased, the initial current increase is followed by a current decrease soon after stirring is stopped. This indicates that not only the local glucose concentration in the brushes is probably significantly lower than in the bulk solution, but even decreasing during the measurement period after stirring. This is in contradiction to the conditions considered for Michaelis–Menten kinetics, which assumes a substrate concentration high enough that changes due to the activity of the enzymes are negligible over the time scale of the experiment.[31] Still, already at a bulk glucose concentration of 1 µM (see the Supporting Information) a clear current increase with respect to the reference sample is visible, giving a detection limit of 1 µM or lower. A linear extrapolation from 0 to 3 mM yields a comparably low sensitivity of approximately 6 nA cm^{-2} mM^{-1}.[7,9,25] At this point, we would like to underline that the scope of this work is not to present an advanced glucose sensor, but a presentation of our system as a platform for the immobilization and electrical wiring of redox active (bio)molecules.

Still, the good signal to-noise-ratio (e.g., ≈10:1 at 3 mM) of our system enables the detection of relevant glucose levels

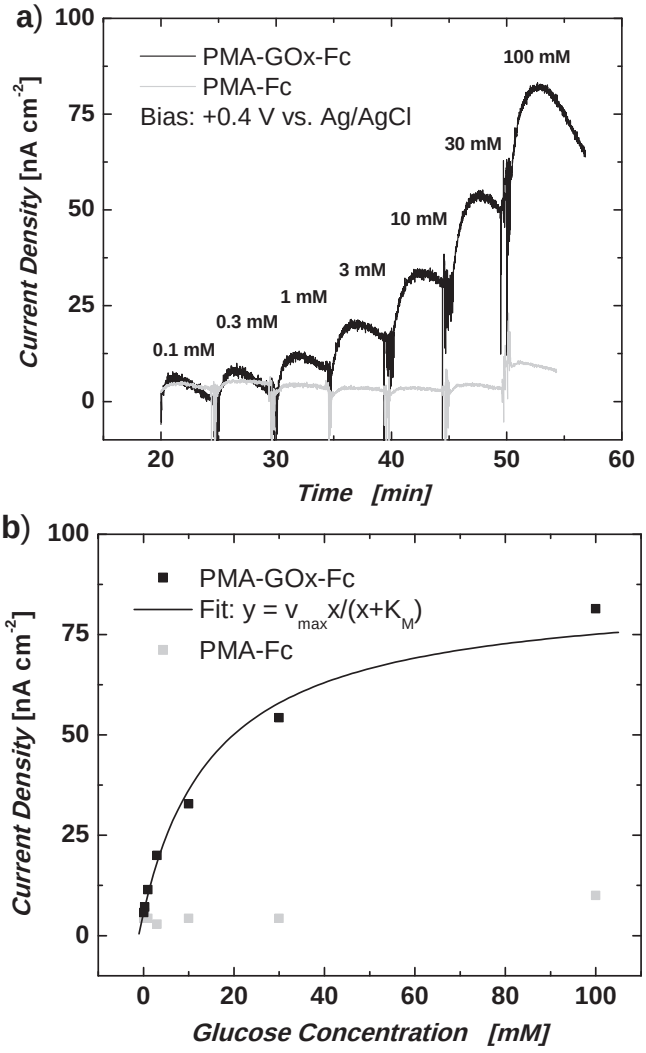

Figure 5. a) Amperometric detection of glucose using GOx-Fc-modified polymer brushes on diamond. Electrons from the oxidation of glucose by GOx generate a concentration dependent current, while the reference sample (without GOx) shows no significant response b) Peak current density vs β-D-glucose concentration (symbols). Hyperbolic fit (solid line) based on Michaelis–Mentenkinetics.

despite the relatively low current densities. Typical glucose concentrations in human blood or the interstitial fluid are usually around 5 mM.[40]

3. Conclusions

Ferrocene and glucose oxidase were successfully immobilized in poly(methacrylic acid) brushes. XPS and cyclic voltammetry indicate high loading of Fc and very efficient electron transfer. Samples were stable over several weeks in aqueous environment due to the strong covalent coupling of PMA, Fc, and GOx. After some initial loss of physisorbed material, no further reduction of the ferrocene concentration is observed even after thorough rinsing or ultrasonication in good solvents. Electrochemical

amperometry and a homovanillic acid assay both show the catalytic activity of GOx. The relatively low performance is attributed mainly to strong constraints on diffusion in the polymer brushes. Thus, reducing the density of the brushes as well as oriented coupling of the enzymes could significantly improve the performance of the system. If a reduction in the grafting density should lead to problems with non-specific adsorption of proteins on the electrode surface, the protein resistance of the brushes could be conserved by first polymerizing a thin but dense layer and then a second less dense brush on top.

On the other hand, the efficiency of the charge transfer, which was studied in comparably high detail, outperforms most similar systems, even if we compare to those with the highest reported sensitivities.[7,9,25] The superior electrochemical properties of diamond allow measurements over a wide potential range and at very low background currents. Overall, functionalized polymer brushes on diamond electrodes offer an interesting strategy for the immobilization and electrical wiring of biomolecules due to the straightforward polymerization process, the high stability and biocompatibility of the brushes, as well as the efficient electrical connection between biomolecules and the electrode in combination with high loading capacities.

4. Experimental Section

Diamond Substrate Growth: Highly doped p-type silicon wafers were cleaned in boiling ammonium hydroxide and hydrogen peroxide (1:1:5 parts DI water at 80 °C) and then in boiling hydrochloric acid and hydrogen peroxide (1:1:5 parts DI water at 80 °C), followed by rinsing with DI water. Subsequently, the silicon wafers were immersed in the aqueous nano-diamond colloid, rinsed with DI water and blown dry with nitrogen. Diamond growth was done in an Astex 6500 series microwave plasma-enhanced chemical vapor deposition reactor. The temperature was monitored with a Williamson Pro92 dual wavelength pyrometer. Growth conditions were: 4% methane in hydrogen, 6500 ppm trimethylboron, 55 mbar process pressure, 3500 W microwave power, 700 °C substrate temperature, process time 20 min, followed by cool down in pure hydrogen plasma.[41,42] Characterization of the NCD films yielded a thickness of 250 nm, with a surface roughness of 10 nm RMS (measured on 5 µm × 5 µm), a boron concentration of the order of 10^{21} cm^{-3} and a conductivity of 50 S cm^{-1}.[43]

NCD substrates were oxidized by boiling in 96% sulfuric acid for 30 min, then thoroughly rinsed with DI water. The chemical oxidation was followed by a 5 min exposure to oxygen plasma in a 100-E Technics Plasma system at 200 W microwave power and 1.4 mbar oxygen pressure.

Self-initiated Photografting and Photopolymerization of PMA: NCD substrates were immersed in about 1 mL of distilled and degassed monomer in a photoreaction tube under dry argon atmosphere and constant irradiation with UV light (300–400 nm, maximum at 350 nm) at RT for 8 h. Excess material was removed by ultrasonication in dichloromethane (DCM), ethyl acetate, and ethanol (all HPLC grade). Deprotection of the carboxylic acid groups was performed by hydrolyzation of the *tert*-butyl groups in methanesulfonic acid and dichloromethane (1:100) at 25 °C for 30 min followed by ultrasonication in DCM, DI water, and ethanol.

Activation of the Pendant Carboxylic Acid Functional Groups of the Polymer Brushes: This was performed in an aqueous solution of 400 mM 1-ethyl-3-(3-dimethylaminopropyl)carbodiimid (EDC) and 100 mM *N*-hydroxysuccinimide (NHS) for 1 hour. After thorough rinsing with buffer solution (40 mM PBS, pH = 7.0), the activated samples were immediately transferred into the respective mediator or enzyme solution.

Polymer Analogue Coupling of Aminomethyl Ferrocene into PMA Brushes: NHS/EDC-activated PMA-modified samples were immersed in a 1 mg mL^{-1} aminomethyl ferrocene solution. Usually, the coupling of aminomethyl ferrocene was performed in acetonitrile (due to a better solubility). However, identical results were obtained when the coupling was performed in enzyme-compatible conditions by dissolving aminomethyl ferrocene in PBS (40 mM, pH = 7.0). The coupling was allowed to complete over night (although already coupling times of around one hour showed a saturation of Fc loading) and the samples were finally cleaned by ultrasonication in acetonitrile, ethyl acetate and ethanol.

Coupling of Glucose Oxidase into PMA Brushes: NHS/EDC-activated PMA-modified samples were immersed in a 1 mg mL^{-1} solution of glucose oxidase from *Aspergillus niger* (purchased from Sigma- Aldrich) in PBS (40 mM, pH = 7.0) over night. Samples were then cleaned by rinsing with buffer, shaking in buffer for one hour, and rinsing with buffer again.

Parallel Coupling of Enzymes and Aminomethyl Ferrocenes into PMA Brushes: NHS/EDC-activated PMA-modified samples were immersed in a 1 mg mL^{-1} solution of GOx in PBS for the enzyme coupling reaction. After one hour the samples were taken out of the GOx solution and immersed in a 1 mg mL^{-1} solution of aminomethyl ferrocene in order to saturate the remaining NHS-ester moieties with Fc. After 3.5 h, the samples were thoroughly rinsed with buffer and further cleaned by shaking in buffer for one hour, and rinsing with buffer again.

Atomic Force Microscopy: Scans were acquired with a Nanoscope IIIa MultiMode scanning probe microscope from Veeco Instruments in an air-conditioned room. Scanners 5298 J and 5308 E as well as standard AFM tips from Veeco were used. All topographic scans were performed in tapping mode. The recorded data was analyzed and visualized with Nanoscope III (Digital Instruments) and WSxM (Nanotec).[44]

X-Ray Photoelectron Spectroscopy: Measurements were performed with a prototype XPS system at a base pressure of 1.4×10^{-9} mbar with non-monochromatic Mg K radiation at an operating power of 10 mA at 15 kV. Prior to analysis, the samples were outgassed for 24 h in a preparation chamber at a base pressure of 5×10^{-10} mbar. Photoelectron core-level spectra were acquired using a hemispherical electron energy analyzer (Specs PCV 300 detection unit) at a pass-energy of 50 eV with a 0.025 eV step size. The spectrometer was calibrated against a C1s binding energy of 284.43 eV.[27]

Electrochemical Experiments: Experiments were performed in a custom-made three electrode electrochemical cell controlled by a Gamry Ref 600 potentiostat. A commercial Ag/AgCl electrode (DriRef-5SH from World Precision Instruments, 3 M KCl, 0.210 V vs. standard hydrogen electrode) served as potential reference and a platinum wire as counter electrode. The cell volume was filled with 20 mL electrolyte (10 mM PBS with 2.7 mM KCl and 137 mM NaCl; pH 7.4 at 25 °C; from Sigma-Aldrich) and kept under an overpressure of nitrogen (after extensive purging with nitrogen prior to the measurements). To obtain β-D-glucose an aqueous solution of α-D-glucose (from Sigma-Aldrich) was prepared. Over a time scale of several hours at room temperature the ratio of β to α isomers equilibrates around 0.64/ 0.36 due to mutarotation and the anomeric effect.[45,46]

Supporting Information

Supporting Information is available from the Wiley Online Library or from the author.

Acknowledgements

This work has been funded by the International Graduate School of Science and Engineering, Project 2.12, the Deutsche Forschungsgemeinschaft, Project GA 1432/1-1, and the Nanosystems Initiative Munich.

Received: August 16, 2012
Revised: November 26, 2012
Published online: January 16, 2013

[1] A. Härtl, E. Schmich, J. A. Garrido, J. Hernando, S. C. R. Catharino, S. Walter, P. Feulner, A. Kromka, D. Steinmueller, M. Stutzmann, *Nat. Mater.* **2004**, *3*, 736.
[2] N. Yang, H. Uetsuka, C. E. Nebel, *Adv. Funct. Mater.* **2009**, *19*, 887.
[3] A. Kraft, *Int. J. Electrochem. Sci.* **2007**, *2*, 355.
[4] C. Popov, W. Kulisch, J. Reithmaier, T. Dostalova, M. Jelinek, N. Ansprach, C. Hammann, *Diam. Relat. Mater.* **2007**, *16*, 735.
[5] J. Rubio-Retama, J. Hernando, B. Lopez-Ruiz, A. Härtl, D. Steinmueller, M. Stutzmann, E. Lopez-Cabarcos, J. A. Garrido, *Langmuir* **2006**, *22*, 5837.
[6] C. E. Nebel, B. Rezek, D. Shin, H. Uetsuka, N. Yang, *J. Phys. D: Appl. Phys.* **2007**, *40*, 6443.
[7] S. A. Merchant, T. O. Tran, M. T. Meredith, T. C. Cline, D. T. Glatzhofer, D. W. Schmidtke, *Langmuir* **2009**, *25*, 7736.
[8] M. Senel, E. Cevik, F. Abasiyanik, *Sens. Actuators, B* **2010**, *145*, 444.
[9] J. Wang, N. V. Myung, M. Yun, H. G. Monbouquette, *J. Electroanal. Chem.* **2005**, *575*, 139.
[10] O. Azzaroni, *J. Polym. Sci., Part A: Polym. Chem.* **2012**, *50*, 3225.
[11] R. Barbey, L. Lavanant, D. Paripovic, N. Schüwer, C. Sugnaux, S. Tugulu, H. Klok, *Chem. Rev.* **2009**, *109*, 5437.
[12] N. A. Hutter, M. Steenackers A. A. Reitinger, O. A. Williams, J. A. Garrido, R. Jordan, *Soft Matter* **2011**, *7*, 4861.
[13] N. A. Hutter, A. A. Reitinger, N. Zhang M. Steenackers O. A. Williams, J. A. Garrido, R. Jordan, *Phys. Chem. Chem. Phys.* **2010**, *12*, 4360.
[14] M. Steenackers, S. Q. Lud, M. Niedermeier, P. Bruno, D. M. Gruen, P. Feulner, M. Stutzmann, J. A. Garrido, R. Jordan, *J. Am. Chem. Soc.* **2007**, *129*, 15655.
[15] M. Steenackers, R. Jordan, A. Küller, M. Grunze, *Adv. Mater.* **2009**, *21*, 2921.
[16] M. Steenackers, A. M. Gigler, N. Zhang, F. Deubel, M. Seifert, L. H. Hess, C. Haley, Y. X. Lim, K. P. Loh, J. A. Garrido, R. Jordan, M. Stutzmann, I. D. Sharp, *J. Am. Chem. Soc.* **2011**, *133*, 10490.
[17] M. Steenackers, I. D. Sharp, K. Larsson, N. A. Hutter, M. Stutzmann, R. Jordan, *Chem. Mater.* **2010**, *22*, 272.
[18] T. Chen, I. Amin, R. Jordan, *Chem. Soc. Rev.* **2012**, *41*, 3280.
[19] X. Lin, Q. He, J. Li, *Chem. Soc. Rev.* **2012**, *41*, 3584.
[20] W. Senaratne, L. Andruzzi, C. K. Ober, *Biomacromolecules* **2005**, *6*, 2427.
[21] R. Hoffmann, A. Kriele, S. Kopta, W. Smirnov, N. Yang, C. E. Nebel, *Phys. Status Solidi A* **2010**, *207*, 2073.
[22] E. Katz et al. in *Encyclopedia of Electrochemistry*, Vol. *9* (Eds: A. J. Bard, M. Stratmann, G. S. Wilson), John Wiley & Sons, New York **2002**, 559.
[23] R. Wilson, A. P. Turner, *Biosens. Bioelectron.* **1992**, *7*, 165.
[24] P. Si, S. Ding, J. Yuan, X. W. Lou, D. Kim, *ACS Nano* **2011**, *5*, 7617.
[25] Z. B. Zhang, S. J. Yuan, X. L. Zhu, K. G. Neoh, E. T. Kang, *Biosens. Bioelectron.* **2010**, *25*, 1102.
[26] D. A. Shirley, *Phys Rev. B* **1972**, *5*, 4709.
[27] NIST X-ray Photoelectron Spectroscopy Database, Version 3.5, http://srdata.nist.gov/xps/(accessed January 2012).
[28] Empirically Derived Atomic Sensitivity Factors for XPS, http://www.uksaf.org/data/sfactors.html (accessed January 2012).
[29] XPS Reference Pages, http://www.xpsfitting.com/2009/04/relative-sensitivity-factors-rsf.html (accessed January 2012).
[30] G. C. Guilbault, P. Jr. Brignac, M. Zimmer, *Anal. Chem.* **1966**, *38*, 190.
[31] W. W. Chen, M. Niepel, P. K. Sorger, *Genes Dev.* **2010**, *24*, 1861.
[32] F. Takusagawa T. F. Koetzle, *Acta Cryst.* **1979**, *35*, 1074.
[33] A. J. Bard, L. R. Faulkner, *Electrochemical Methods: Fundamentals and Applications*. John Wiley & Sons, New York **2001**.
[34] E. A. Laviron, *J. Electroanal. Chem.* **1980**, *112*, 1.
[35] E. F. Dalton, N. A. Supridge, J. C. Jernigan, K. O. Wilbourn, J. S. Facci, R. W. Murray, *J. Chem. Phys.* **1990**, *141*, 143.
[36] S. W. Feldberg, I. Rubinstein, *J. Electroanal. Chem.* **1988**, *240*, 1.
[37] I. Fritsch-Faules, L. R. Faulkner, *J. Electroanal. Chem.* **1989**, *263*, 237.
[38] B. Aussedat, M. Dupire-Angel, R. Gifford, J. C. Klein, G. Reach, *Am. J. Physiol. Endocrinol. Metab.* **2000**, *278*, 716.
[39] P. He, X. Chen, *J. Electroanal. Chem.* **1988**, *256*, 353.
[40] V. Leskovac, S. Trivic, G. Wohlfahrt, J. Kandrac, D. Pericin, *Int. J. Biochem. Cell. Biol.* **2005**, *37*, 731.
[41] O. A. Williams, O. Douhéret, M. Daenen, K. Haenen, E. Osawa, M. Takahashi, *Chem. Phys. Lett.* **2007**, *445*, 255.
[42] M. Daenen, O. A. Williams, J. D'Haen, K. Haenen, M. Nesládek, *Phys. Status Solidi A* **2006**, *203*, 3005.
[43] W. Gajewski, O. A. Williams, P. Achatz, K. Haenen, E. Bustarret, M. Stutzmann, J. A. Garrido, *Phys. Rev. B* **2009**, *79*, 045206.
[44] I. Horcas, R. Fernandez, J. M. Gomez-Rodriguez, J. Colchero, J. Gomez-Herrero, A. M. Baro, *Rev. Sci. Instrum.* **2007**, *78*, 013705.
[45] J. E. McMurry, *Organic Chemistry*. Brooks/Cole Pub. Co., Pacific Grove, USA **1987**, 866.
[46] E. Juaristi, G. Cuevas, *The Anomeric Effect*. CRC Press, Boca Raton, USA **1995**, 9.